INDI 1 TC

DEMANDE D'AUTORISATION N°
EN VUE D'UNE PUBLICATION OU D'UNE COMMUNICATION

Direction : ....

Centre : ....

Réf émetteur : ....

9400 1574

NIG n° 316

Titre original du document : EXPERIMENTAL AND THERMODYNAMIC ASSESSMENTS OF SUBSTITUTIONS IN THE AlFeSi, FeMnSi, FeSiZr and AlCaFeSi SYSTEMS (65 wt.% Si) SOLIDIFICATION SIMULATION.

Titre traduit en anglais : —

Titre traduit en français : Détermination expérimentale et par le calcul de substitutions dans les systèmes AlFeSi FeMnSi FeSiZr et AlCaFeSi (65 m.%Si). Simulation de la solidification –

AUTEURS	AFFILIATION [1]	DEPT/SERV/SECT	VISA (d'un des auteurs)	DATE
GUENEAU CHRISTINE	CEA/ DCC	DPE / SPEA / SEPC	C. Guéneau	15/09/94

Nature du document [2] : CEA-CONF--

PERIODIQUE	CONF/CONGRES	POSTER	RAPPORT	THESE	COURS	MEMOIRE DE STAGE	Chapitre d'OUVRAGE
☐	☒	☐	☐	☐	☐	☐	☐

Pièces jointes : RÉSUMÉ ☐ TEXTE ☒

CONGRES / CONFERENCE — Nom : Material's Week 94 — Ville : Rosemont — Pays : USA — Date du : 2/10/94 au 6/10/94 — Organisateur : TMS

PERIODIQUE — Titre : — Comité de lecture : oui ☐ non ☐

OUVRAGE — Titre : — Éditeur :

THESE / MEMOIRE DE STAGE / COURS — Université / Établissement d'enseignement :

ARRIVE LE 14 MAR. 1995 SBDS / SPRI

DOMAINES :

LANGUE :

N° EPAC :

SUPPORT : Disquette ☐ Papier ☐

MOTS-CLES : THERMODYNAMIC - AlFeSi - FeMnSi - FeSiZr - AlCaFeSi - Ferrosilicon - SOLIDIFICATION

Les visas portés ci-dessous attestent que la qualité scientifique et technique de la publication proposée a été vérifiée et que la présente publication ne divulgue pas d'information brevetable, commercialement utilisable ou classée.

	SIGLE	NOM	DATE	VISA	OBSERVATIONS	REF
CHEF DE SERVICE	SPEA	DECAUDON	28.9.94	P.i		
CHEF DE DEPARTEMENT	DPE	V. LAPIERRE				
		J. CAZALET	6/10/94			
		R. HAGEMANN	7/10/94			

ARRIVEE - CIRST 13 OCT. 94 005838 Circ. : Cit. :

Date limite d'envoi du résumé : .... Date limite d'envoi du texte : .... Date limite d'envoi du poster : ../../..

Destinataires :

Les correspondants publication des départements se chargent de transmettre à l'INSTN/MIST/CIRST (Saclay) copies des demandes d'autorisation de publication, du résumé et du texte définitif.

EXPERIMENTAL AND THERMODYNAMIC ASSESSEMENTS OF SUBSTITUTIONS IN THE AlFeSi, FeMnSi, FeSiZz and AlCaFeSi SYSTEMS (65 wt % Si) - SOLIDIFICATION SIMULATION.

Christine Guéneau°,*, Colette Servant* and Ibrahim Ansara"

* Laboratoire de Métallurgie Structurale, URA CNRS 1107, Université de Paris-Sud, 91405 Orsay-Cedex, France.

° Laboratoire Central de Recherche de Chedde, Société Péchiney-Electrométallurgie, 74190 Le Fayet, France.

" Laboratoire de Thermodynamique et de Physicochimie Métallurgiques, URA CNRS 29, ENSEEG, B.P. 75, 38402, Saint-Martin d'Hères, France.

Abstract

The subsitutions of Al<->Si, Fe<->Mn and Fe<->Zr in some intermetallic compounds of the Al-Fe-Si, Fe-Mn-Si and Fe-Si-Zr systems were modelled in the Si-rich corner using a two sublattice model. The solidification paths of the studied alloys were determined at equilibrium. The as calculated phase volume fractions of the alloys were compared to the experimental ones. Finally, a solidification simulation using the Gulliver-Scheil's model was performed in order to explain the formation of some precipitates experimentally observed.

Introduction

High purity ferrosilicon alloys of Péchiney Electrométallurgie (PEM) with 65 wt % Si are used either as cast iron inoculants with small amounts of alloying elements (Al, Ca, Mn, Zr...) or in the elaboration of magnetic thin sheets. The material is produced by reduction of scrap silica by carbon in presence of iron; the as obtained ingot is then ground in order to obtain granula. During this process, ferrosilicon alloys generate an important quantity of undesirable small size particles (Φ<200µm), called "fines". In order to understand this grinding behaviour, the alloy microstructure has been studied (1). In fact, the nature and the composition of the different phases which precipitate, can affect mechanical properties. The material is constituted of two major phases: silicon plates embedded in a matrix of leboite $Si_{2.4}Fe$. Several percentages of alloying elements as Al, Ca, Mn and Zr either substitute - for silicon or iron - in the matrix, or take part in the formation of minor other phases. For interpreting and modelling these various observed microstructures as a function of the alloy composition, it was necessary to determine the alloy solidification sequences. Phase diagrams have been calculated using the thermodynamic properties of all the phases, derived from the minimization of the Gibbs energy of the system. In addition, the Gulliver-Scheil's model, integrated in the Thermo-Calc data-bank (2) has been applied to simulate solidification for ingot cooling process.

Material

In order to study the respective influence of each alloying element, ternary model alloys Al-Fe-Si, Fe-Mn-Si and Fe-Zr-Si with 65 wt % Si and 1 to 4 wt % of alloying element as well as a quaternary model alloy Al-Ca-Fe-Si with 65 Si, 1 Al and 1 Ca in wt % were elaborated by PEM. An industrial high purity alloy Fe-Si with 65 wt % Si , called 65HP, was used as a reference. The ternary alloys have been prepared by melting that alloy in which the pure alloying element was added. The chemical analysis of all these alloys are indicated in Table I.

Table I . Chemical analysis of the studied alloys in wt. %.

Alloy	Si	Fe	Ca	Al	Mn	Zr
65HP	64.6	34.2	0.073	0.12	0.12	0.008
1Al	66.1	31.8	0.15	0.96	0.11	0.007
1.5Al	65.1	32.0	0.078	1.53	0.11	0.006
4Al	64.9	30.7	0.05	4.11	0.13	0.018
4Zr	65.5	30.3	0.15	0.022	0.12	3.65
4Mn	64.4	31.2	0.02	0.022	4.08	0.350
1Ca1Al	65.2	31.4	1.71	1.05	0.19	0.017

Experimental Data

The as solidified ingot microstructure was observed using a LEICA 260 scanning electron microscope. The phase composition was measured with a CAMEBAX electron microprobe. The phase volume percentages were determined by three experimental methods: i) chemical analysis (1); ii) nuclear neutron diffraction experiments. These tests were made on powder specimens with a high resolution diffractometer (λ=2.426Å). The Rietveld profile refinement procedure was applied in order to calculate the phase volume fractions; this method consists in fitting the calculated spectra from the known phase crystalline structures to the experimental data (intensity versus diffraction angle) (1). Previously, it was necessary to determine the crystalline structure of some intermetallic compounds such as: Al_3FeSi_2 and $Al_3Fe_2Si_3$ by X-ray diffraction (3, 4); iii) image analysis. This method was applied on back-scattered electron images treated by the Optilab program. These experiments have not been carried out on the 1Ca1Al alloy because of the complexity of its microstructure .

Thermodynamic modelling

The thermodynamic properties of the various phases existing in the different ternary and quaternary systems were derived from a least-square optimization procedure using experimental phase diagram and thermodynamic data. For all thermodynamic calculations, the procedures developed by Lukas et al (5) or PARROT available in Thermo-Calc software worked out by Jansson (6) were used.

Phase diagram and thermodynamic data

Al-Fe-Si and Al-Ca-Fe-Si systems

The phase diagram of the quaternary Al-Ca-Fe-Si system has been calculated in the Si-rich corner by Anglézio et al (7, 8); these authors did not take into account the different (Al<->Si) substitutions in the phases $(Si,Al)_{2.4}Fe$ and $FeAl_3Si_2$. Previous thermodynamic calculations were performed using Anglézio's database in order to determine the solidification paths of our alloys (9). Our experimental data concerning the three alloys 1Al, 1.5Al and 4Al are reported on the isothermal section given in Figure 1, and compared to the results of Anglézio et al (7, 8) and Zarechnyuk et al (10). A maximum solubility of aluminium for silicon in the matrix $(Si,Al)_{2.4}Fe$ equal to about 10 at.% was measured: this result is in good agreement with the values of Anglézio et al (7, 8) and Zarechnyuk et al (10). The limits of the composition range of Al_3FeSi_2 vary with the authors (Figure 1). In addition, thermodynamic parameters of the compound $Al_9Fe_2Si_2$ were optimized.

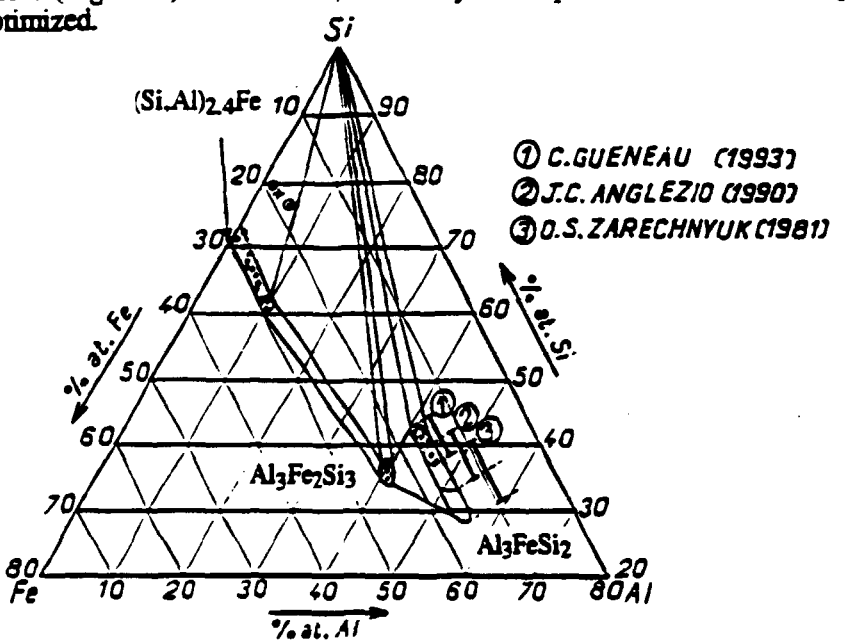

Figure 1 - Isothermal section Al-Fe-Si presenting the experimental measurements of both $(Si,Al)_{2.4}Fe$ and Al_3FeSi_2 chemical composition.

Fe-Mn-Si system:

The thermodynamic data used in this study are those calculated by Forsberg et al (11). These authors did not take into account the (Fe<->Mn) substitutions in the Si-rich corner of the system. The maximum content of manganese in the matrix $Si_{2.4}(Fe,Mn)$ we have measured, is equal to about 4.6 at. %.

Fe-Si-Zr system:

The two binary Fe-Zr and Si-Zr systems were recently assessed (12, 13). Several authors (14, 15, 16) have reported the existence of numerous ternary intermetallic compounds. In a first step, these ternary compounds have not been taken into account in the present study. Furthermore, a maximum content of 6.9 at. % iron was measured in the $Si_2(Zr,Fe)$ compound; this value is slightly higher than the one, (5 at.% at 800°C), obtained by Lysenko et al (17).

Substitution modelling

The pure solid elements at 298.15K in their stable form were chosen as the reference state of the system. For the thermodynamic functions of the pure elements in their stable and metastable state, the SGTE phase stability equations published by Dinsdale (17) were used. The equations as a function of temperature are given in the following form:

$$^{\circ}G_i(T) - H_i^{SER}(298.15K) = a + b.T + c.T.\ln(T) + d.T^2 + e.T^{-1} + f.T^3 + i.T^7 + j.T^{-9} \quad (1)$$

The stability of the phases is described relative to the standard elements reference (SER) at 298.15K. In binary systems, the solid solutions were represented by the polynomial Redlich-Kistler model (18):

$$G^{\phi} - H^{SER} = {}^{ref}G^{\phi} + {}^{id}G^{\phi} + {}^{E}G^{\phi} \quad (2)$$

where

$${}^{ref}G^{\phi} = \sum x_i.\left[{}^{\circ}G_i^{ref}(T) - H_i^{SER}(298.15K)\right] \quad (3)$$

$${}^{id}G^{\phi} = R.T.\left[\sum x_i.\ln(x_i)\right] \quad (4)$$

$${}^{E}G^{\phi} = x_i.x_j.[{}^{\circ}L^{\phi} + {}^{1}L^{\phi}.(x_i - x_j) + ...] \quad (5)$$

$$with\ {}^{k}L^{\phi} = a_k + b_k.T + c_k.T.\ln(T) + ...$$

The Gibbs energy excess terms of the ternary solid solutions are described as a function of the binary interaction parameters of the three different systems. A ternary interaction parameter α can be included as follows:

$${}^{E}G_{ijk}^{\phi}(T) = \sum_{i=1}^{j-1}\sum_{j=i+1}^{3} x_i.x_j.{}^{E}G_{ij}(T) + \prod_{k=1}^{3} x_k.\alpha \quad (i \neq j) \quad (6)$$

The stoichiometric solid phases are expressed as a function of the temperature as follows:

$$G^{\phi} - H_i^{SER}(298.15K) = a + b.T + c.T.\ln(T) + d.T^2 + e.T^{-1} + f.T^3 \quad (7)$$

The intermetallic compounds $(Si,Al)_{2.4}Fe$, $Si_{2.4}(Fe,Mn)$ and $Si_2(Zr,Fe)$, which exhibit a range of non stoichiometry, were modelled using a two-sublattice model. The Gibbs energy of formation of a compound $A_p(B_{y''B},C_{y''C})_q$, per formula unit, is then equal to

$$G^{\phi} - H^{SER} = {}^{ref}G^{\phi} + {}^{id}G^{\phi} + {}^{E}G^{\phi} \quad (8)$$

where

$${}^{ref}G^{\phi} = [y''_B.{}^{\circ}G^{\phi}_{A:B} + y''_C.{}^{\circ}G^{\phi}_{A:C}] \quad (9)$$

$${}^{id}G^{\phi} = R.T.q.[y''_B.\ln(y''_B) + y''_C.\ln(y''_C)] \quad (10)$$

$${}^{E}G^{\phi} = [y''_B.y''_C.{}^{\circ}L^{\phi}_{A:B,C}] \quad (11)$$

as y''_B and y''_C are respectively the site fractions of B, C in the second sublattice designated by ". The term ${}^{\circ}L^{\Phi}_{A,B,C}$ represents the interaction energy between the two species on the second sublattice ".The composition range of the Al_3FeSi_2 phase was modelled considering the compound $Fe(Al,Si)_5$. The thermodynamic description of this phase is the same that the above ones.

The optimized parameters of these four phases in addition to the ones of the $Al_9Fe_2Si_2$ stoichiometric compound are given in Table II.

Figures 2 to 5 represent the isothermal sections of the ternary systems Al-Fe-Si (at 873 K and 1173 K), Fe-Mn-Si (at 1473K) and Fe-Si-Zr (at 1073K); each one shows the domains of solubility of the above phases. The composition range of Al_3FeSi_2 derived from calculation is narrower than the experimental one. This can be explained by the simplicity of the two sublattice model involved and by the lack of experimental data. These results could be improved by introducing other interaction terms in the model.

Solidification simulation

Two ways of calculation of the alloy solidification paths were applied:

- the first possibility is to consider that during solidification the overall composition does not vary.
- the second one is to apply the Gulliver-Scheil's model where the following conditions are assumed: i) there is a local equilibrium at the solid/liquid interfaces; ii) the liquid is homogeneous and iii) there is no diffusion in the solid phases. So the fraction of the solid phase which precipitates will no longer participate in the solidification process (2). During solidification, a long as a two-phase equilibrium takes place, the overall composition of the system is continously modified until a third phase precipitates. In this case, the composition of the liquid will follow a three or multiphase line until no liquid remains. The simulation of the solidification was performed by considering stepping in temperature.

Figure 6 shows the microstructure of the 65HP reference alloy, composed of two major phases: silicon plates in a $Si_{2.4}Fe$ matrix. The eutectoid transformation ($Si_{2.4}Fe$ -> Si_2Fe + Si) does not occur in our alloys because of an important cooling rate. Then, the low temperature form of the leboite Si_2Fe was thus not considered during the solidification simulation calculations.

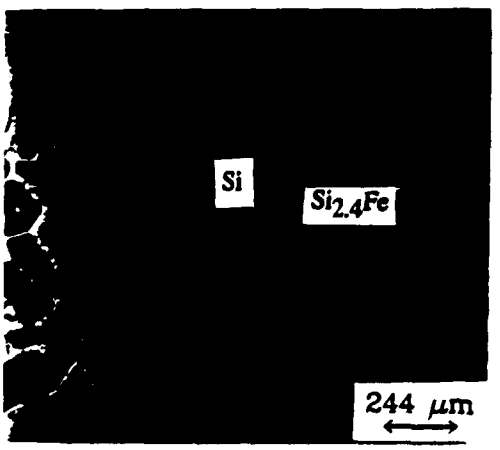

Figure 6 - Electron micrograph of the 65HP reference alloy.

Table III presents the phase volume fractions determined both by Thermo-Calc calculations and by several experimental methods. It shows a general good agreement between the various methods for the 65HP reference. The low value of the silicon percentage, determined by image analysis, is due to its lamellar morphology.

Tables IV to VI give the experimental and calculated volume fractions as a function of the composition for the different ternary alloys. The absence of Si_2Fe in these alloys and the high measured solubility of the elements in the different phases signify that the structure is quenched. In order to take it into account, the calculations of the phase volume fraction by Thermo-Calc were performed at a temperature above the eutectoid reaction one, as indicated in Tables IV to VI. The agreement is very satisfactory between the results obtained by the various methods. Figures 7 to 10 represent isopleths of the systems Al-Fe-Si, Fe-Mn-Si, Fe-Si-Zr and Al-Ca-Fe-Si showing the alloy solidification paths at equilibrium conditions.

Table II . Optimized thermodynamic parameters of the phases.

Phase	Thermodynamic properties (J/mol)
$(Si,Al)_{2.4}Fe$	$G^0(T)-.7H_{Si}^{0,diamond}-.3H_{Fe}^{0,bcc-A2}= -19649-0.92T+.7GHSER_{Si}+.3GHSER_{Fe}$ $G^0(T)-.7H_{Al}^{0,fcc-Al}-.3H_{Fe}^{0,bcc-A2}=-11693.4+3.5T+.7\ GHSER_{Al}+.3\ GHSER_{Fe}$ $L^{0,(Si,Al)_{2.4}Fe}= -10415.1$
$(Si,Al)_2Fe$	$G^0(T)-.67H_{Si}^{0,diamond}-.33H_{Fe}^{0,bcc-A2}= -27383+3.48T+.67GHSER_{Si}+.33GHSER_{Fe}$ $G^0(T)-.67H_{Al}^{0,fcc-Al}-.33H_{Fe}^{0,bcc-A2}=-23000+3.48T+.67GHSER_{Al}+.33GHSER_{Fe}$
Al_3Si_2Fe	$G^0(T)-.83H_{Al}^{0,fcc-Al}-.17H_{Fe}^{0,bcc-A2}=-28000+24T+.83GHSER_{Al}+.17GHSER_{Fe}$ $G^0(T)-.83H_{Si}^{0,diamond}-.17H_{Fe}^{0,bcc-A2}=-18500+25T+.83GHSER_{Si}+.17GHSER_{Fe}$ $L^{0,(Si,Al)_3Fe}=-72000+T$
$Al_9Fe_2Si_2$	$G^0(T)-.692H_{Al}^{0,fcc-Al}-.154H_{Fe}^{0,bcc-A2}-.154H_{Si}^{0,diamond}=-38000+17T+.692GHSER_{Al}$ $+.154GHSER_{Fe}+.154GHSER_{Si}$
$Si_{2.4}(Fe,Mn)$	$G^0(T)-.3H_{Fe}^{0,bcc-A2}-.7H_{Si}^{0,diamond}=-19649-0.92T+.3\ GHSER_{Fe}+.7GHSER_{Si}$ $G^0(T)-.3H_{Mn}^{0,cbcc-A2}-.7H_{Si}^{0,diamond}-12901.3-0.0922T+.3GHSER_{Mn}+.7GHSER_{Si}$
$Si_2(Fe,Mn)$	$G^0(T)-.33H_{Fe}^{0,bcc-A2}-.67H_{Si}^{0,diamond}=-27383+3.48T+.33GHSER_{Fe}+.67GHSER_{Si}$ $G^0(T)-.33H_{Mn}^{0,cbcc-A2}-.67H_{Si}^{0,diamond}=-17000+3.48T+.33GHSER_{Mn}+.67GHSER_{Si}$
$Si_2(Fe,Zr)$	$G^0(T)\ -2H_{Si}^{0,diamond}-H_{Zr}^{0,hcp-A3}=-189332.2+354.9T-63.2T\ln(T)-0.00768T^2$ $+139751.1T^{-1}-1.972.10^{-11}T^3$ $G^0(T)-2H_{Si}^{0,diamond}-H_{Fe}^{0,bcc-A2}=-56686.4+353.T-63T\ln(T)$

Table III - Calculated and experimental phase volume fractions for the 65HP reference alloy.

Alloy	Phase	Vol. % (1)	Vol. % (2)	Surf.% (3)	Vol. % (4)
65HP	Si	45.0 ± 1.0	44.5	46.8 ± 4.1	41.7
	$Si_{2.4}Fe$	55.0 ± 0.9	55.5	52.6 ± 4.4	58.3

(1) determined from neutron diffraction experiments. (2) calculated from chemical analysis (performed by PEM).
(3) determined by image analysis. (4) calculated by Thermo-Calc.

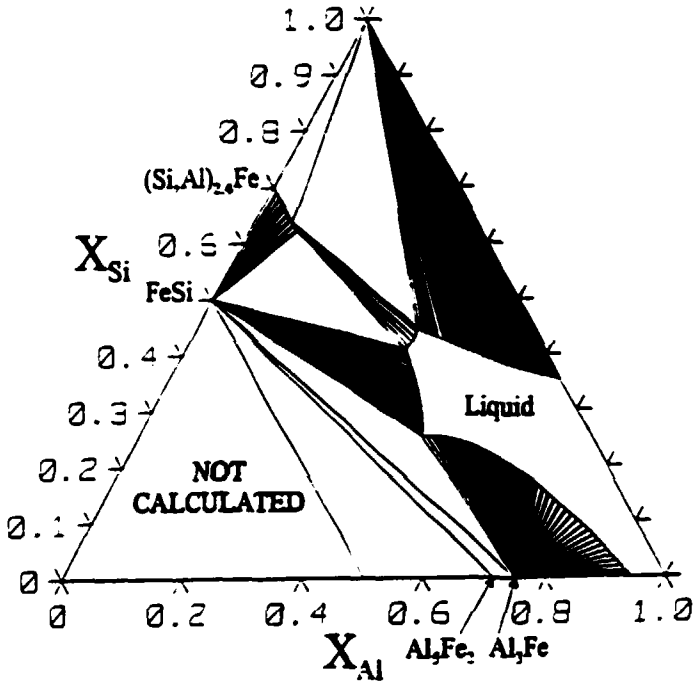

Figure 2 - Al-Fe-Si isothermal section at 1173 K showing the maximum solubility of aluminium in $(Si,Al)_{2.4}Fe$.

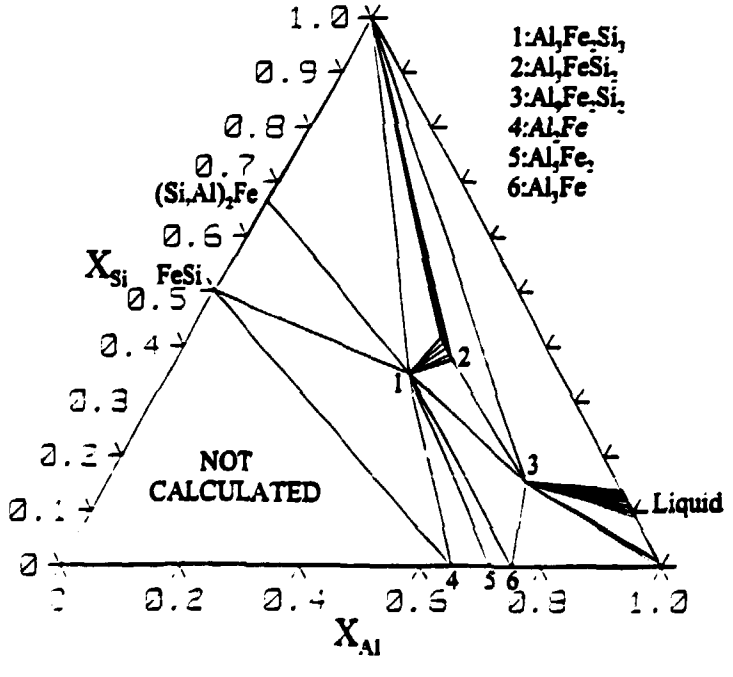

Figure 3 - Al-Fe-Si isothermal section at 873 K showing the composition range of Al_3FeSi_2.

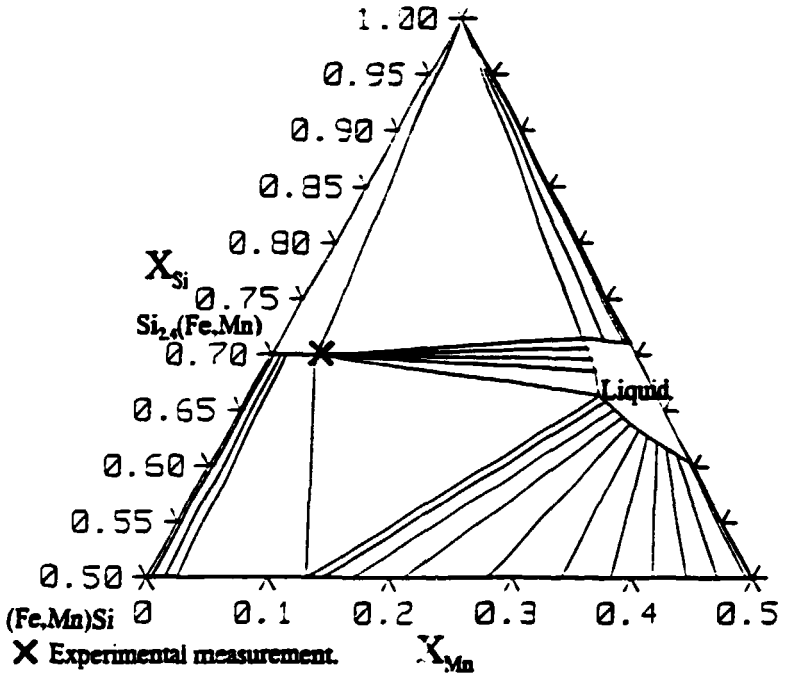

Figure 4 - Fe-Mn-Si isothermal section at 1473 K showing the maximum solubility of manganese in $Si_{2.4}(Fe,Mn)$.

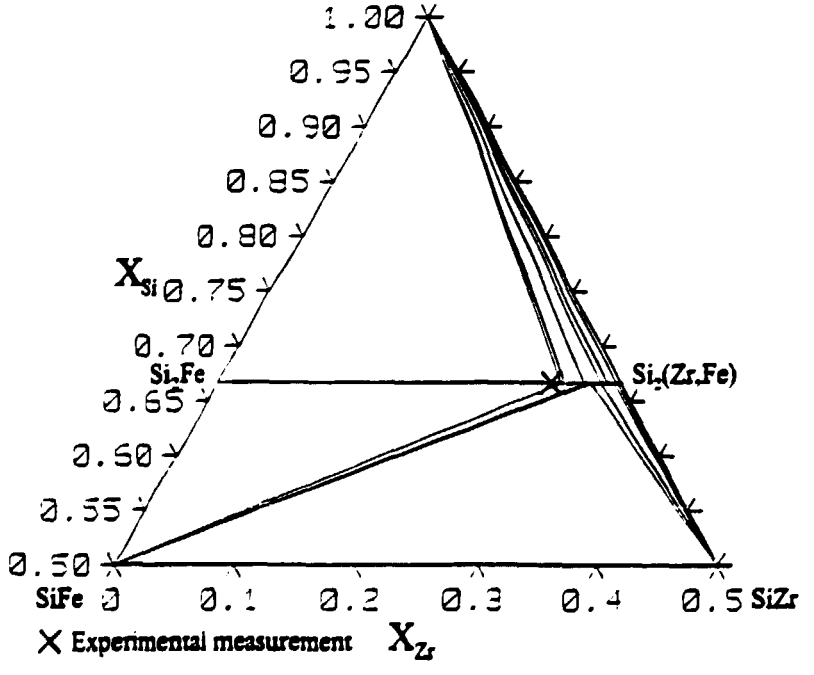

Figure 5 - Fe-Si-Zr isothermal section at 1073 K showing the maximum solubility of iron in $Si_2(Zr,Fe)$.

Table IV - Calculated (at 850°C) and experimental phase volume fractions for the 1Al. 1.5Al and 4Alalloys.

Alloy	Phase	Vol. % (1)	Vol. % (3)
1Al	Si	47.2 ± 1.2	51.6
	$(Si,Al)_{2.4}Fe$	51.5 ± 1.0	48.4
	Al_3FeSi_2	0.6±0.2	-
	$Al_3Fe_2Si_3$	0.6 ± 0.1	-
1.5Al	Si	46.4 ± 1.4	51.1
	$(Si,Al)_{2.4}Fe$	52.3 ± 1.1	48.9
	Al_3FeSi_2	0.4 ± 0.2	-
	$Al_3Fe_2Si_3$	0.8±0.2	-
4Al	Si	49.9 ± 1.3	52.9
	$(Si,Al)_{2.4}Fe$	45.5 ± 0.9	41.8
	Al_3FeSi_2	0.9 ± 0.2	-
	$Al_3Fe_2Si_3$	3.6 ± 0.2	5.2

Table V - Calculated (at 1000°C) and experimental phase volume fractions for the 4Mn alloy.

Alloy	Phase	Vol. % (1)	Vol. % (2)	Vol. % (3)	Surf. % (4)
4Mn	Si	33.5 ± 0.9	35.4	41.3	28.8 ± 4.0
	$Si_{2.4}(Fe,Mn)$	66.5 ± 1.0	64.6	58.7	70.8 ± 3.9

Table VI - Calculated (at 1000°C) and experimental phase volume fractions for the 4Zr alloy.

Alloy	Phase	Vol. % (1)	Vol. % (2)	Vol. % (3)	Surf. % (4)
4Zr	Si	37.8 ± 1.0	42.7	48.5	36.7 ± 4.0
	$Si_{2.4}Fe$	55.6 ± 1.1	52.4	47.4	47.5 ± 3.7
	$Si_2(Zr,Fe)$	6.6 ± 0.4	4.9	4.1	14.7 ± 1.8

(1) determined from neutron diffraction experiments.
(2) calculated from chemical analysis (performed by the PEM Society).
(3) calculated by Thermo-Calc. (4) determined by image analysis.

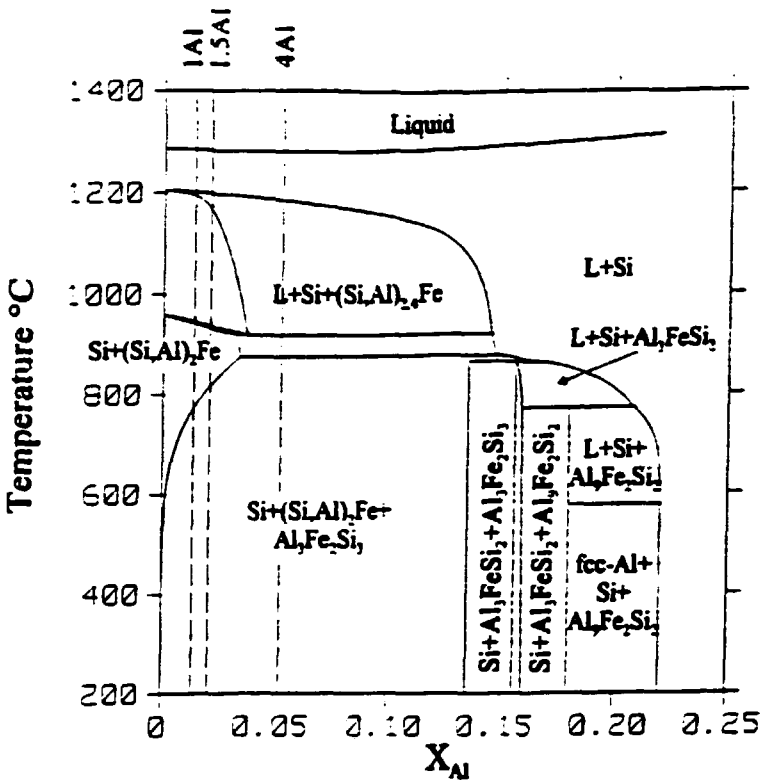

Figure 7 - Al-Fe-Si isopleth with x(Si)=.8, showing the solidification paths of the 1Al, 1.5Al and 4Al alloys.

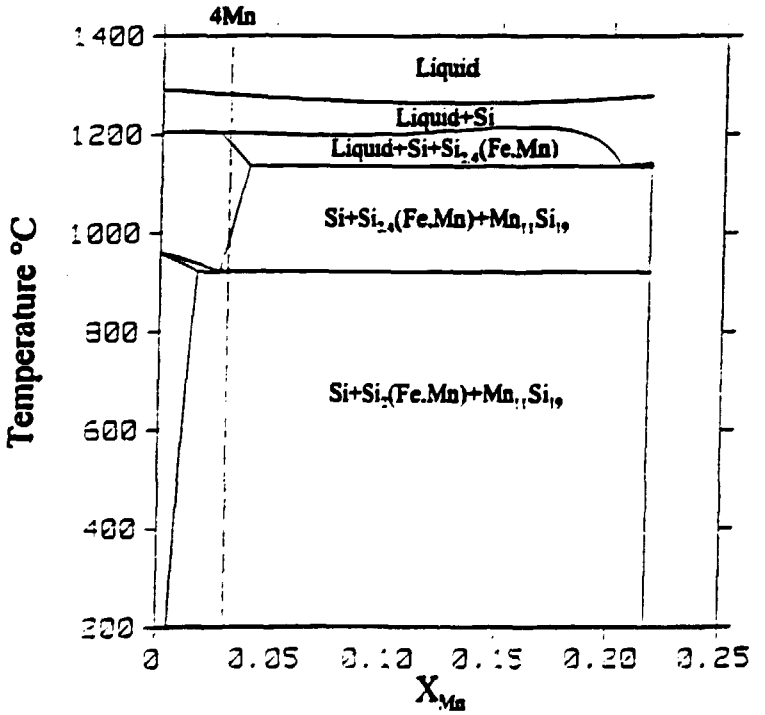

Figure 8 - Fe-Mn-Si isopleth with x(Si)=.783, showing the solidification path of the 4Mn alloy.

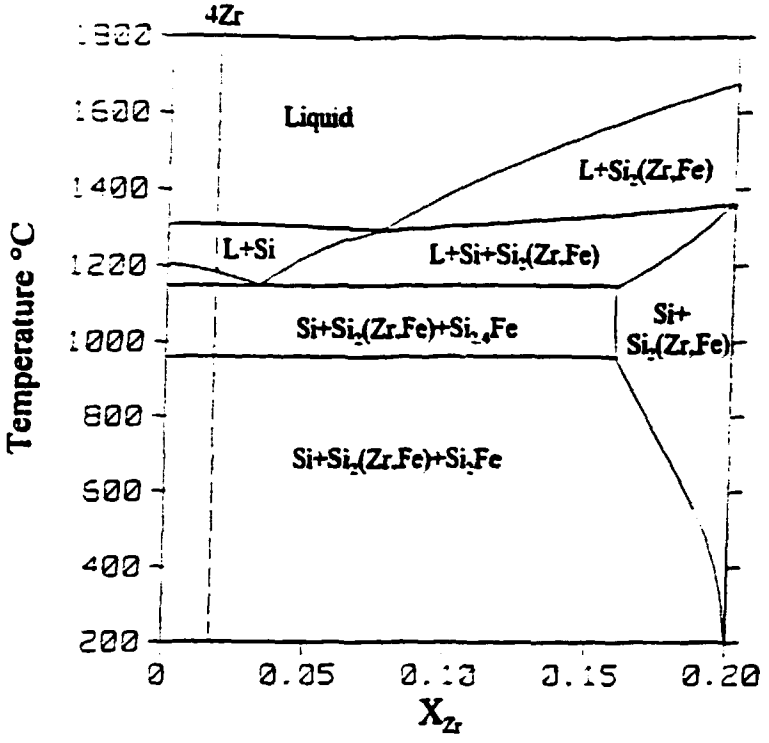

Figure 9 - Fe-Si-Zr isopleth with x(Si)=.8, showing the solidification path of the 4Zr alloy.

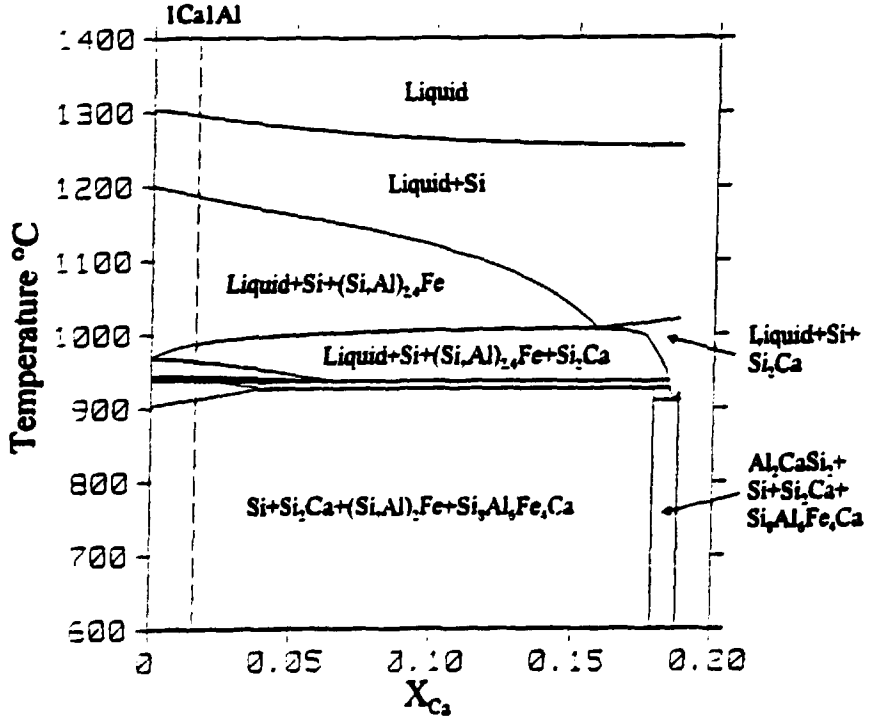

Figure 10 - Al-Ca-Fe-Si isopleth with x(Si)=.8 and x(Al)=.013, showing the solidification path of the 1Ca1Al alloy.

The micrographs of the 1.5Al, 4Mn, 4Zr and 1Ca1Al alloys are presented in the following figure:

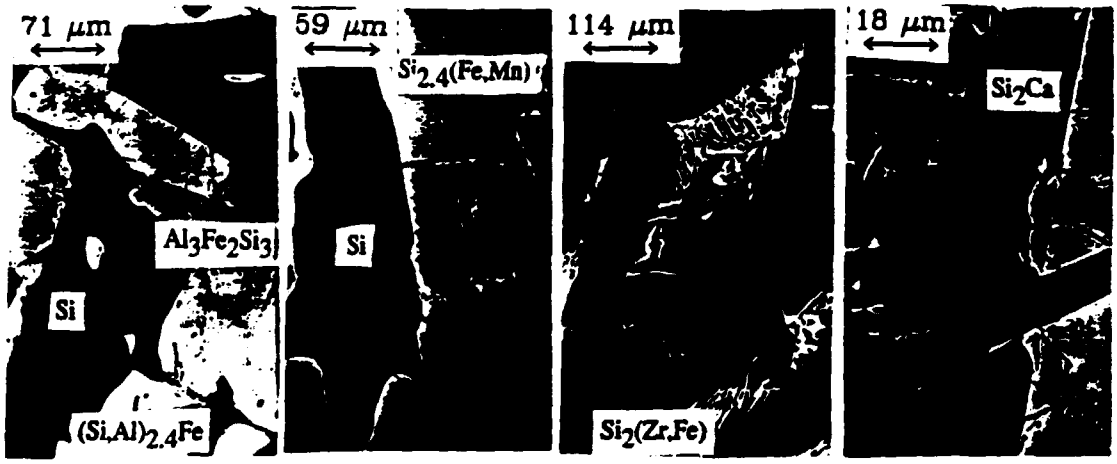

Figure 11 - Electron micrographs of the 1.5Al (a), 4Mn (b), 4Zr (c) and 1Ca1Al (d) alloys.

Al-Fe-Si

Experimentally, aluminium is concentrated both in the matrix and in two intermetallic ternary compounds Al_3FeSi_2 and $Al_3Fe_2Si_3$ (Fig.11a). The solidification simulation in equilibrium conditions shows the absence of Al_3FeSi_2 in the (Al,Fe,Si) alloys considered (Fig. 7). In the case of the 1Al and 1.5Al alloys, the silicon plates first solidify. A binary eutectic reaction gives rise to the formation of the high temperature form of leboite and secondary crystallized silicon. Then, both phases lead to the formation of $Al_3Fe_2Si_3$ as observed on Figure 11a. For the 4Al, first silicon plates solidify, then the binary eutectic reaction takes place and finally the very low quantity of remaining liquid transforms in the high temperature form of leboite, ternary silicon and $Al_3Fe_2Si_3$ during a ternary eutectic reaction. By considering the proximity of the compositions of both ternary compounds, it can be assumed that a little variation of the liquid composition could explain the precipitation of Al_3FeSi_2. The simulation using the Gulliver-Scheil's model is in good agreement with the experimental results; in fact it predicts the precipitation of the Al_3FeSi_2 phase as observed on Figure 12 which represents the evolution of the liquid mole fraction as a function of the temperature using the two ways of calculation.

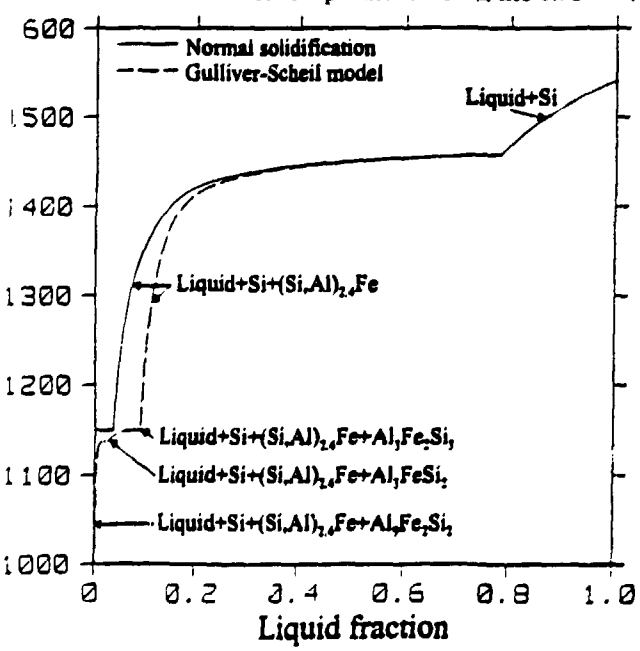

Figure 12 - Liquid fraction as a function of temperature, calculated either at equilibrium (__) or using the Gulliver-Scheil's model (---), for the 4Al alloy.

In the case of the following systems and except for Al-Ca-Fe-Si, the results of the Gulliver-Scheil simulation are not given in the present paper because the observed phases correspond to the ones obtained in the equilibrium condition calculations.

Fe-Mn-Si

The solidification path of the 4Mn alloy is shown in Figure 8. During cooling, Mn is first concentrated in $Si_{2.4}(Fe,Mn)$, then in $Mn_{11}Si_{19}$ which precipitates as follows: $Si_{2.4}(Fe,Mn)$ -> $Si + Mn_{11}Si_{19}$. Experimentally, the observed volume fraction of $Mn_{11}Si_{19}$ was very low (Figure 11b); so the observed alloy microstructure corresponds to the one calculated at about 1000°C.

Fe-Si-Zr

The solidification path of the 4Zr alloy is given in Figure 9. Zr is concentrated in $Si_2(Zr,Fe)$ which forms during a ternary eutectic reaction, experimentally verified by the morphology of the microstructure (Figure 11c). The volume fraction of the $Si_2(Zr,Fe)$ precipitates is overestimated by image analysis because of their fineness.

Al-Ca-Fe-Si

Experimentally, the major phases Si, $(Si,Al)_{2.4}Fe$, Si_2Ca were observed as well as a low quantity of $Si_8Al_6Fe_4Ca$ and Si_2Al_2Ca in the 1Ca1Al alloy (Figure 11d). The solidification simulation at equilibrium conditions does not predict the formation of Si_2Al_2Ca (Figure 10). The presence of this compound can be explained by a composition variation of the liquid as verified by the Gulliver-Scheil simulation (Figure 13).

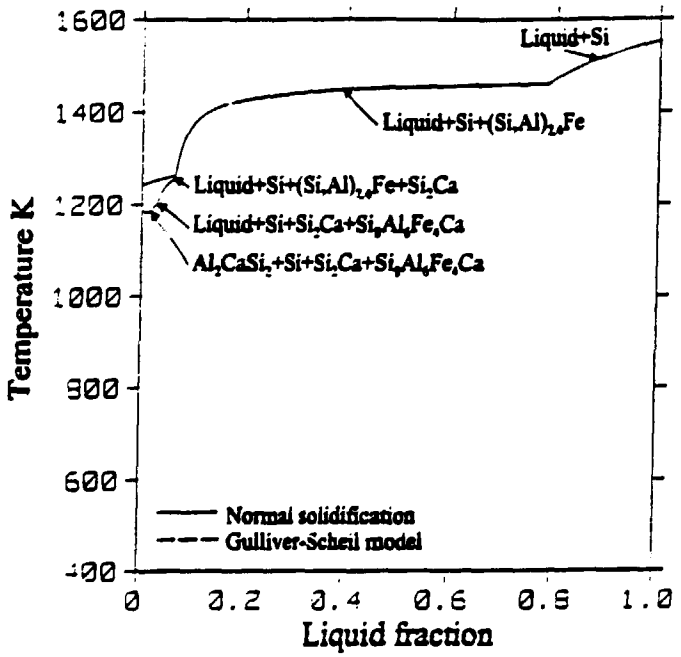

Figure 13 - Liquid fraction versus temperature for the 1Ca1Al alloy, calculated at equilibrium (__) or using the Gulliver-Scheil's model (---).

Correlation with the mechanical properties of the material

This study has allowed both to simulate the alloy solidification and to quantify the phase volume fraction. These last results were correlated with the mechanical properties. Grindability tests and grinding simulation have been undertaken in order to study the influence of the ferrosilicon chemical composition (1,19). Figure 14 gives the evolution of the percentage of the fines as a function of the $Si_{2.4}Fe$ volume fraction for a fine grinding procedure. A slight increase in the percentage of fines with the matrix quantity is observed. The study of the alloy microstructure

has permitted to interpret this evolution. The microstructure analysis has revealed the presence of a crack net in the $Si_{2,4}Fe$ matrix; the size of the grains delineated by these cracks is very close to the one of the fines, about several hundred microns. Thermomechanical stresses may be responsible for this crack net formation which can explain the important fine production. The influence of each alloying element has been determined.

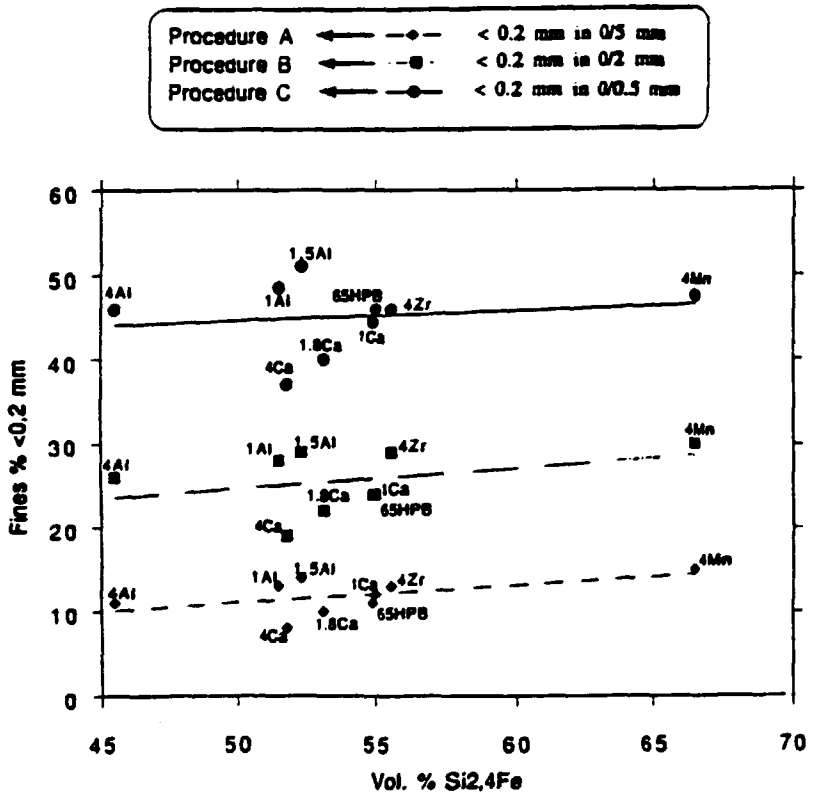

Figure 14 - Fine percentage versus volume fraction of $Si_{2,4}Fe$ for all studied alloys.

Conclusion

The present study, including the consideration of the element substitution in the intermetallic compounds of our alloys, has led to the assessment of databases concerning ferrosilicon systems which allows to simulate the alloy solidification, to quantify the phase amount, then to modify their elaboration process in order to improve the mechanical properties of the alloys. A satisfactory agreement was found between calculations and experiments.

References

1. C. Guéneau, "Etude de la mécanique de fracture de ferro-alliages en relation avec leur macro et microstructure" Thèse de Doctorat en Sciences, Université de Paris Sud, Orsay, (1993).

2. B. Sundman, B. Jansson and J.-O. Andersson, "The Thermo-Calc Databank System", Calphad, 2 (9) (1985), 153-190.

3. C. Guéneau, C. Servant and F. d'Yvoire, "Structure of $FeAl_3Si_2$", Acta Crystallographica, to be published.

4. C. Guéneau, C. Servant and F. d'Yvoire, "Structure of $Fe_2Al_3Si_3$", Acta Crystallographica, to be submitted.

5. H.L. Lukas, J. Weiss and E.-Th. Henig,"Strategies for the calculation of Phase Diagrams", Calphad, 6 (3) (1982) 229-251.

6. B. Jansson, "Computer Operated Methods for Equilibrium Calculations and Evaluation of Thermochemical Model Parameters", Ph.D. Thesis, KTH, Stockholm, Sweden (1983).

7. J.-C. Anglézio, C. Servant and I. Ansara, "Contribution to the Experimental and Thermodynamic Assessment of the Al-Ca-Fe-Si System - I. Al-Ca-Fe, Al-Ca-Si, Al-Fe-Si and Ca-Fe-Si Systems", Calphad, 18 (3) (1994) 273-302.

8. J.-C. Anglézio, C. Servant and I. Ansara , "A study of the Si-rich Domain of the Al-Ca-Fe-Si Quaternary System", Calphad, 18 (3) (1994) 303-318.

9. C. Guéneau, C. Servant and I. Ansara, "Solidification-microstructure relationships of model ferro-silicon alloy by means of thermodynamic calculations of ternary (Al,Fe,Si) and (Ca,Fe,Si) phase diagrams", J. de Chimie Physique, 90, 2 (1992) 399-407.

10. O.S. Zarechnyuk, N.V. German, T.I. Yanson. R.M. Rykhal and A.A. Muraveva,"Some phase diagrams of aluminium with transition metals, rare earth metals and silicon", Fazovye Ravnovesiya, Met. Splavakh. (1981) 69-73.

11. A. Forsberg and J. Agren ,"Thermodynamic Evaluation of the Fe-Mn-Si System and the γ/ε Martensitic Transformation", J. of Phase Equilibria, 14, 3 (1993) 354-363.

12. C. Guéneau , C. Servant and I. Ansara, "Thermodynamic Assessment of the Si-Zr System", Calphad, 18, 3 (1994) 319-327.

13. C. Servant, C. Guéneau and I. Ansara, "Experimental and Thermodynamic Assessment of the Fe-Zr System", J. of Alloys and Compounds, to be published.

14. P. Chaudouet, B.Lambert, R. Madar and R. Fruchart, "Existence d'une phase G dans le ternaire Fe-Zr-Si", Annales de Chimie, 9, 2 (1984) 119-121.

15. YA.P. Yarmolyuk, L.A. Lysenko and E.I. Gladyshevskii, "Crystal structure of new ternary compounds in the zirconium-iron-silicon system", Tezisy Dokl. - Vses. Konf. Kristallokhim. Intermet. Soedin. 2nd, Ed. R.M. Rykhal (L'VOV. GOS. UNIV., LVOV, USSR, 1974).

16. L.A. Lysenko, Z. Ban, YA.P. Yarmolyuk and E.I. Gladyshevskii, "Reaction of zirconium with iron group transition metlas and silicon", Strukt. Faz. Fazovye Prevrashch. Diagr. Sostoyaniya Met. Sist. (1974) 21-25.

17. A.T. Dinsdale, "SGTE Data for pure elements", Calphad, 15 (4) (1991) 317-425.

18. O. Redlich and A. Kister, "Algebraic Representation of Thermodynamic Properties and the Classification of Solutions", Ind. Eng. Chem., 40 (1948) 345-348.

19. C. Guéneau, C. Servant and F.Manier, "Relationships between the grinding behaviour and the microstructure of ferro-silicon alloys with 65 wt. % silicon" (Paper presented at the 7th International Ferroalloy Conference INFACON7, Trondheim, Norway, June 1995).